




Inclined magnetized and energy transportation aspect of infinite shear rate viscosity model of Carreau nanofluid with multiple features over wedge geometry

Syed Zahir Hussain Shah¹  | Irwan Fathurrochman² | Assad Ayub¹  | Gilder Cieza Altamirano³  | Ali Rizwan⁴ | Rafaél Artidoro Sandoval Núñez³ | Zulqurnain Sabir¹ | Manshuk Yeskindirova⁵

¹Department of Mathematics and Statistics, Hazara University, Mansehra, Pakistan

²Department of Islamic Educational Management, Institut Agama Islam Negeri Curup, Rejang Lebong, Indonesia

³Department of General Studies, National Autonomous University of Chota, Chota, Perú

⁴Department of Industrial Engineering, King Abdulaziz University, Jeddah, Saudi Arabia

⁵Translation Theory and Practice Department, L.N. Gumilyov Eurasian National University, Astana, Kazakhstan

Correspondence

Assad Ayub, Department of Mathematics and Statistics, Hazara University, Mansehra 21300, Pakistan.
Email: assadayub610@yahoo.com

Abstract

Heat transference in fluid mechanism has a deep influence in real-life applications like hot-mix paving, recovery of energy, concrete heating, heat spacing, refineries, distillation, autoclaves, reactors, air conditioning, and so forth. In this attempt, findings related to energy exchange with features of infinite shear rate viscosity model of Carreau nanofluid by placing inclined magnetic dipole over the wedge are made. The main role in the transportation of heat is exercised by incorporating facts of radiation, nonuniform heat sink source, Brownian motion, thermophoresis, and chemical reaction. The mathematical system of the infinite shear rate viscosity model of Carreau nanofluid gives a system of partial differential equations and furthermore, these are moved into ordinary differential equations. A numerical procedure is applied via shooting/bvp4c to obtain numerical results. Inclined magnetic dipole gives a lower velocity of Carreau nanofluid. Due to the relaxation time factor velocity of Carreau fluid gets down. A^* causes to generate the heat internally, so due to this, temperature increases

rapidly. The increasing rate of temperature is found very high for the growing Hartmann number. The rate of mass transport becomes low for gradual increment in the parameter of thermophoresis, wedge angle, and Prandtl. Inclined magnetic dipole gives a lower velocity of Carreau nanofluid. Due to the relaxation time factor, the velocity of the Carreau fluid goes down. The absence and presence of magnetic numbers have no influence on velocity, temperature, and concentration files for Le , R_d , θ_f , γ , We , β , Pr , Nb , Nt , A .

KEYWORDS

Brownian motion, Carreau nanofluid, inclined magnetic dipole, infinite shear rate viscosity, wedge geometry

1 | INTRODUCTION

The Carreau fluid model gave an extra dimension to researchers to investigate the characteristics of fluid flow at very low and very high shear rates. This capability of the Carreau fluid is distinguished from other models like Casson, Maxwell, power-law, and other non-Newtonian models because these models are just capable in the power-law region. Many researchers have focused on this model and extensive literature is found regarding the Carreau fluid.^{1–3} Recently Khan et al.⁴ made a study related to the numerical analysis of Carreau fluid flow with analysis of Fourier's and Fick's laws. In this article, many real-life applications of Carreau fluid are listed, such as engineering, petroleum, nuclear safety process, and so forth. Over geometry of variable thickness melting surface with attached Cattaneo–Christov heat flux conditions is treated by Ramadevi et al.⁵ He also examined the magnetic effect with heat transport. Nazir et al.⁶ started studying the phenomenon of radiative heat flux with the mathematical model of the Carreau model. Concentration and its relationship with Fick's law and Carreau fluid flow due to normal surface condition is described by Khan et al.⁷ Heat transfer effects on electro-magnetohydrodynamic Carreau fluid flow between two microparallel plates and convection in nanofluids and induced magnetic field on peristaltic pumping are discussed in Refs. [8,9].

Due to the immense consumption of heat at industrial or other levels, thermal science gets worries.

Thermal management is trying to reduce this extra consumption with the help of nanotechnology. Researchers^{10–19} found that energy can be increased by using the heat transfer analysis in a nanofluid. Nanofluids are capable of increasing the thermal conductivity of working liquid and thus growth in thermal energy takes place. Transport of heat through nano liquid proved to have extraordinary significance in many real-life applications^{20–29} like allurements comprising chilling of microelectronics, space refrigerating, cancer diagnoses, and treatment, proficiency, drilling, transformers oil cooling, high-powered lasers, nuclear industries, microchips in computer processors, solar systems, and energy capture.

Studies related to magnets have practical influence in real applications like nanofluid pumping, molten salt, molten metal, and pumping of seawater, and due to its significance,

many scholars have presented their studies.^{30,31} Khan et al.³² did an investigation related to change in internal energy by taking mathematical viscosity of Carreau fluid along with the basic facts of Ohmic heating. For the purpose of biomedical application, Mahanthesh et al.³³ made their analysis about the magnetohydrodynamic flow of Carreau liquid over a stretchable sheet with a variable thickness.

Brownian motion is the result of continuous bombardment from molecules and due to this creation of nanoparticles takes place. The random movement of such nanostructure particles is referred to as Brownian motion like dust and smog. It is a microscopic process. Conversely, the phenomenon of disbursement of these particles is called thermophoresis. Their applications are optical process, manufacturing of electrical instruments, separation-related to molecules, and so forth. their description is located in.^{34–37}

Review literature gives a brief explanatory note on Carreau nanofluid, heat transport, MHD flow, Brownian motion, and thermophoresis with different scientific facts which are studied earlier. But there is missing, the combined effect of the inclined magnetic field with infinite shear rate viscosity model of Carreau nanofluid. This missing gap is going to be filled by this study. In this study, the inclined magnetized and energy transportation aspect of the infinite shear rate viscosity model of Carreau nanofluid with multiple features over wedge geometry is taken into consideration.

The rest of this paper consists of several sections: formulation of problem, based on Carreau fluid over the wedge, methodology, proof of the existence of the study, results/discussion, and reaction of physical quantities and their interpretation for Carreau fluid along with seized parameters.

2 | FORMULATION OF PROBLEM BASED ON CARREAU FLUID OVER WEDGE

In this section, there is an assumption made that flow is induced by wedge geometry and fluid is incompressible, unsteady, and a non-Newtonian class of the Carreau model. The aspect of the inclined magnetic field is utilized by placing an inclined magnetic dipole. Exchange of energy is carried out by imposing facts of radiation, nonuniform heat sink source, Brownian motion, thermophoresis, and chemical reaction. The stretchiness of wedge with velocity $U_w = \frac{bx^m}{1-ct}$ induced flow of Carreau fluid. Furthermore, $U_e = \frac{ax^m}{1-ct}$ is the mathematical relationship for free stream velocity of the wedge and m lies in the range of $[0, 1]$. The angle of the wedge is expressed in terms of β and π and denoted as $\Omega = \pi\beta$. $B(t) = \frac{b_0}{\sqrt{1-ct}}$ is imposed magnetic field with an inclination of ω with the surface of the wedge (externally). The x -axis is adopted along with the wedge, and orthogonal to the wedge, the y - axis is taken. It is assumed that $(T_w > T_\infty)$, that is, nonuniform temperature T_w is considered greater than T_∞ and similarly $(C_w > C_\infty)$.

Physical interpretation of formulation is presented in Figure 1.

The governing equations²³ of continuity, momentum, energy, and nano mass transfer can be written as

$$\frac{\partial u}{\partial x} = -\frac{\partial v}{\partial y}, \quad (1)$$

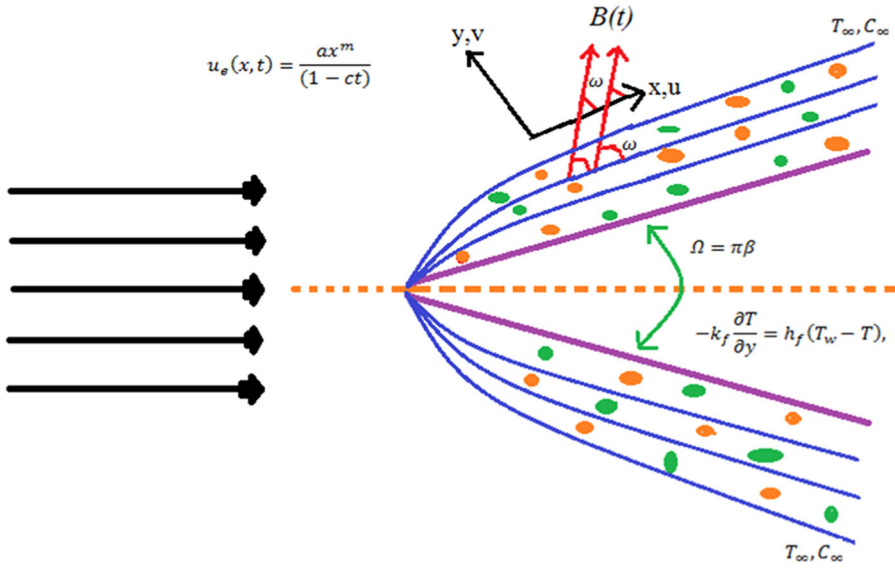


FIGURE 1 Interpretation of physical model for flow [Color figure can be viewed at wileyonlinelibrary.com]

$$\begin{aligned} & \frac{\partial u}{\partial t} + u \frac{\partial u}{\partial x} + v \frac{\partial u}{\partial y} - \frac{\partial U_e}{\partial t} - \frac{dU_e}{dx} \\ & \frac{\partial u}{\partial t} + u \frac{\partial u}{\partial x} + v \frac{\partial u}{\partial y} - \frac{\partial U_e}{\partial t} - \frac{dU_e}{dx} \\ & = \frac{\sigma^* B^2(t)}{\rho} \sin^2(\omega)(U_e - u) + \nu \left[\beta^* \frac{\partial^2 u}{\partial y^2} + (1 - \beta^*) \frac{\partial}{\partial y} \left[\frac{\partial u}{\partial y} \left[1 + \left(\Gamma \frac{\partial u}{\partial y} \right)^2 \right]^{\frac{n-1}{2}} \right] \right], \end{aligned} \quad (2)$$

$$\left[D_B \left(\frac{\partial T}{\partial r} \frac{\partial C}{\partial r} \right) + \frac{D_T}{T_\infty} \left(\frac{\partial T}{\partial r} \right)^2 \right] \tau + \alpha \frac{\partial^2 T}{\partial y^2} - \frac{\partial T}{\partial t} - u \frac{\partial T}{\partial x} - v \frac{\partial T}{\partial y} - \frac{1}{\rho c_p} \frac{\partial q_r}{\partial y} = \frac{q'''}{\rho c_p}, \quad (3)$$

$$D_B \frac{\partial^2 C}{\partial y^2} - \frac{\partial C}{\partial t} - u \frac{\partial C}{\partial x} = v \frac{\partial C}{\partial y} + k_c(C - C_\infty) - \frac{D_T}{T_\infty} \frac{\partial^2 T}{\partial y^2}. \quad (4)$$

Nonuniform heat sink source is shown by the relationship¹³

$$\left(\frac{xv}{kU_w(x)} \right) q''' - [f'A^*T_\infty + B^*T - B^*T_\infty] = 0. \quad (5)$$

With boundary conditions

$$u = U_w(x, t) \Rightarrow u - \lambda_1 U_e = 0, v = 0, -k \frac{\partial T}{\partial y} - h_f(T_w - T) = 0, C - C_w(x, t) = 0 \text{ at } y = 0,$$

u approaches to U_e , T approaches to T_∞ , C approaches to C_∞ , as y approaches to ∞ . (6)

$$U_w(x, t) = bx^m(1 - ct)^{-1}, T_w(x, t) = \frac{v(1 - ct)^{\frac{1}{2}}T_\infty + T_0 U_w x}{v(1 - ct)^{\frac{1}{2}}},$$

where concentration is given as¹³

$$C_w(x, t) = \frac{C_\infty v(1 - ct)^{\frac{1}{2}} + C_0 U_w x}{v(1 - ct)^{\frac{1}{2}}}, U_e(x, t) = (1 - ct)^{-1} ax^m, B(t) = (1 - ct)^{-\frac{1}{2}} B_0. \tag{7}$$

Estimation of heat flux is listed mathematically as

$$q_r = -\frac{16\sigma^*}{k*12} \frac{\partial T^4}{\partial y} = -\frac{64\sigma^* T_\infty}{12k^*} \frac{\partial T}{\partial y}, \tag{8}$$

$$\begin{aligned} \frac{64\sigma^* T_\infty}{12(\rho C)_f k^*} \frac{\partial q_r}{\partial y} + \frac{Q_0}{(\rho C)_f} (T - T_\infty) + \alpha \frac{\partial^2 T}{\partial y^2} - u \frac{\partial T}{\partial x} - v \frac{\partial T}{\partial y} + \frac{\tau D_T}{T_\infty} \left(\frac{\partial y}{\partial t} \right)^{-2} + \frac{\partial T}{\partial t} \\ + \tau D_B \left(\frac{\partial T}{\partial y} \frac{\partial C}{\partial y} \right) = 0. \end{aligned} \tag{9}$$

Considering the stream function as a transformation

$$\begin{aligned} \eta^2 = y^{1/2} (m + 1) (2\nu x)^{-1} u_e, \Psi^2(x, y, t) = \sqrt{f(\eta)} (2\nu (m + 1)^{-1} x u_e) \theta(\eta) \\ = (T - T_\infty) (T_w - T_\infty)^{-1}, \varphi(\eta) = (C - C_\infty) (C_w - C_\infty)^{-1}, \end{aligned} \tag{10}$$

$$\begin{aligned} [ff'' + \{1 - (f')^2\}] + [\beta^* + (1 - \beta^*)(1 + (Wef'')^2)]^{\frac{n-3}{2}} \{1 + n(Wef'')^2\} f''' \\ [ff'' + \{1 - (f')^2\}] + [\beta^* + (1 - \beta^*)(1 + (Wef'')^2)]^{\frac{n-3}{2}} \{1 + n(Wef'')^2\} f''' \\ - [A(2 - \beta)] = -\left(\frac{\eta}{2} f'' + f' - 1\right) + M^2 \sin^2 \omega f', \end{aligned} \tag{11}$$

$$\begin{aligned} \theta'' + Pr(\theta' f - 2f'\theta) - Pr[(A/2)(2 - \beta)(\eta\theta' + 3\theta) + [N_b\theta'\phi' + N_t(\theta')^2]] \\ = -\frac{d}{d\eta} [\{1 + Rd(1 + (\theta_f - 1)\theta)^3\theta'\} - [f'A^* + B^*\theta]], \end{aligned} \tag{12}$$

$$\frac{N_t}{N_b} \theta'' + LePr\delta\phi + \phi'' = -LePr(f\phi' + 2f'\phi) + LePr(A/2)(2 - \beta)(\eta\phi' + 3\phi). \tag{13}$$

Local similarities are attached with Boundary conditions through the following equation:

$$\begin{aligned} f'(\infty) \text{ approaches } 0, f(0) = 0, f'(0) - \lambda_1 = 0, \theta'(0) - \gamma(2 - \beta)^{\frac{1}{2}} \{1 - \theta(0)\} \\ = 0, \theta(\infty) \text{ approaches } 0, \varphi(0) - 1 = 0, \varphi(\infty) \text{ approaches } 0. \end{aligned} \tag{14}$$

3 | REAL-TIME QUANTITIES AND THEIR MATHEMATICAL RELATIONS

$$\frac{C_{fx} \rho U_w}{\tau_w} = 1, \frac{k(T_w - T_\infty) Nu_x}{x q_w} = 1, \frac{Ru_x D_B (C_w - C_\infty)}{x q_w} = 1, \tag{15}$$

where

$$\tau_w = \mu_o \frac{\partial u}{\partial y} \left[\beta^* + (1 - \beta^*) \left(1 + (\Gamma \gamma)^2 \right)^{\frac{n-1}{2}} \right],$$

$$\frac{q_w}{-k \left(\frac{\partial T}{\partial y} \right)_{y=0}} = 1,$$

$$\frac{q_m}{-D_B \left(\frac{\partial C}{\partial y} \right)_{y=0}} = 1.$$

So,

$$Re^{\frac{1}{2}} (2 - \beta)^{\frac{1}{2}} C_{fx} = f'' \left[\beta^* + (1 - \beta^*) \left(1 + (Wef'')^2 \right)^{\frac{n-1}{2}} \right], \tag{16}$$

$$(2 - \beta)^{\frac{1}{2}} Re^{-\frac{1}{2}} Nu_x = -\theta'(0) \left\{ 1 + \frac{4}{3N_R} \left[1 + (\theta_w - 1) \right]^3 \right\}, \tag{17}$$

$$(2 - \beta)^{\frac{1}{2}} Re^{-\frac{1}{2}} Sh_x = -\phi'(0). \tag{18}$$

4 | METHODOLOGY

Nonlinear ODEs along with associated BCs are converted from BVP to IVP and then they are integrated with built-in MATLAB tool `bvp4c`. Thus, ruling ODEs are renovated as first-order ODEs. The procedure of the Matlab program is listed as

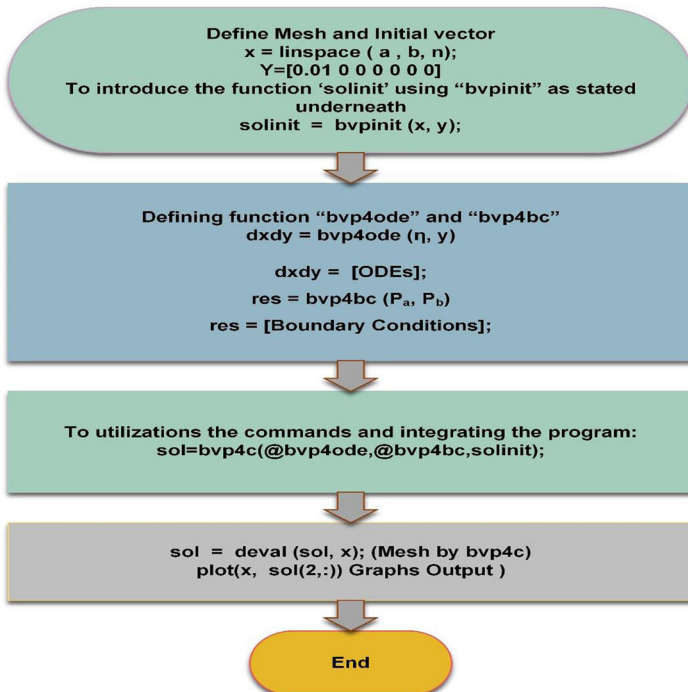


TABLE 1 Substantiation of $\sqrt{Re} C_{fx} (2 - \beta)^{\frac{1}{2}}$ for We

We	Ref. [23]	Present	
	Numeric approach	Approach of Bvp4c	Approach of shooting
0.000	0.59800	0.59934315	0.599321015
0.200	0.63700	0.63832421	0.638211321
0.400	0.68400	0.68985321	0.682239805
0.600	0.72000	0.72932106	0.729332016

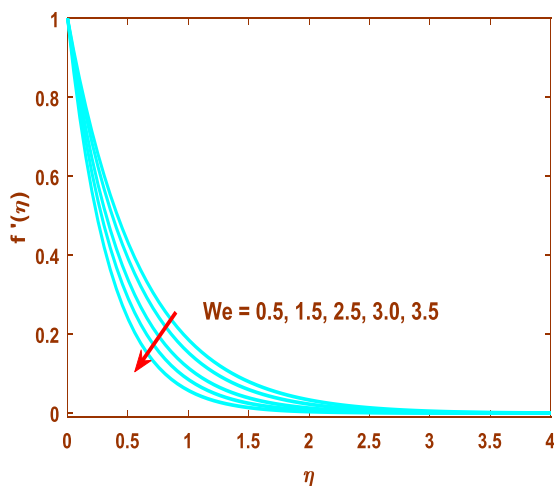


FIGURE 2 Association of We with f' [Color figure can be viewed at wileyonlinelibrary.com]

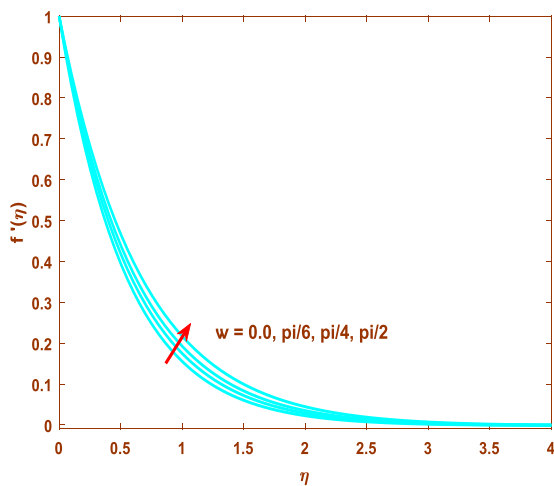


FIGURE 3 Association of ω with f' [Color figure can be viewed at wileyonlinelibrary.com]

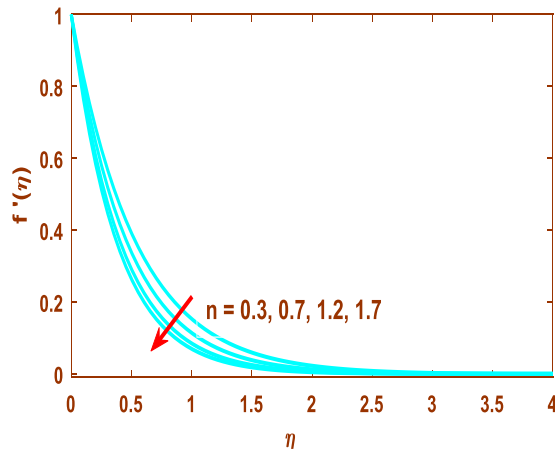


FIGURE 4 f' associated numerically with n [Color figure can be viewed at wileyonlinelibrary.com]

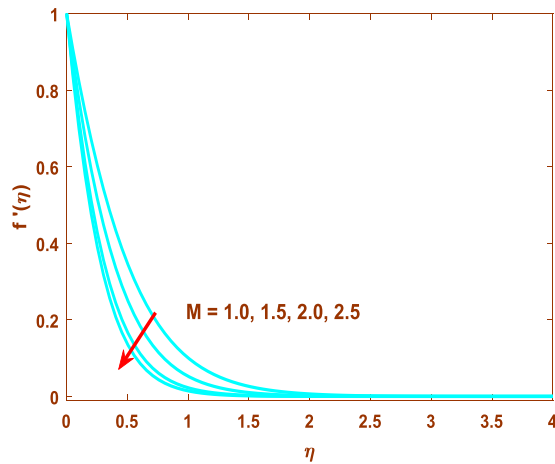


FIGURE 5 f' associated numerically with M [Color figure can be viewed at wileyonlinelibrary.com]

5 | PROOF OF EXISTENCE OF STUDY

Satisfaction of this study is made through Table 1, and quite an agreement is found with old literature.

6 | RESULTS AND DISCUSSION

This section brings all numerical results of velocity, energy, concentration, and all physical quantities with attached parameters through Figures 2–36. Bvpc4c/shooting scheme is adopted to obtain all these numerical results which are very significant to readers. Investigation of influential parameters like Lewis number, radiation parameter, temperature ratio parameter, thermal Biot number, Weissenberg number, wedge angle parameter, Prandtl number,

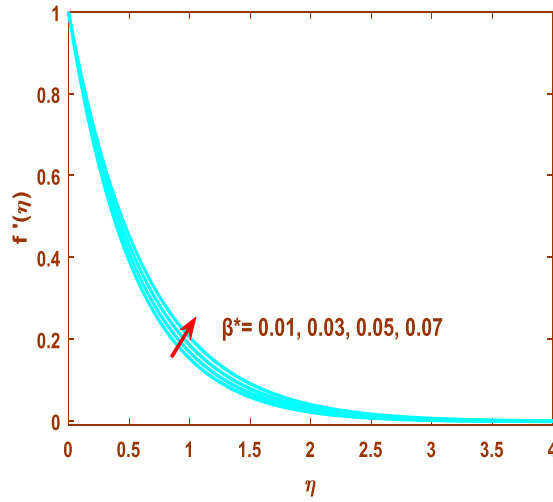


FIGURE 6 f' associated numerically with β^* [Color figure can be viewed at wileyonlinelibrary.com]

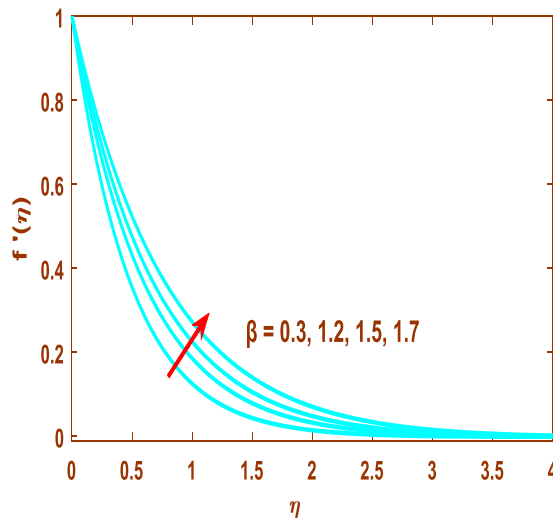


FIGURE 7 f' associated numerically with β [Color figure can be viewed at wileyonlinelibrary.com]

Hartmann number, Brownian movement parameter, thermophoresis parameter, and unsteadiness parameter $Le, R_d, \theta_f, \gamma, We, \beta, Pr, Ha^2, Nb, Nt, A$, overall visibilities of fluid are made through Figure 2–21. Drag forces, Nusselt number, and Sherwood number are scrutinized by statistical sketching through Figures 22–36.

6.1 | Velocity interpretation of Carreau fluid along seized parameters

Figure 2–6 are presented to investigate the comprehensive analysis of seized parameters on velocity interpretation of Carreau fluid. Weissenberg number is seized by relaxation time

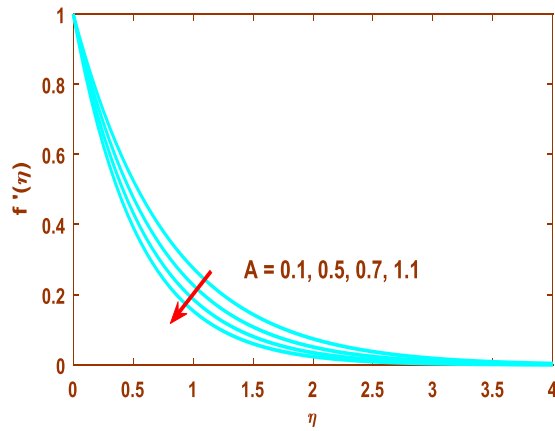


FIGURE 8 f' associated numerically with A [Color figure can be viewed at wileyonlinelibrary.com]

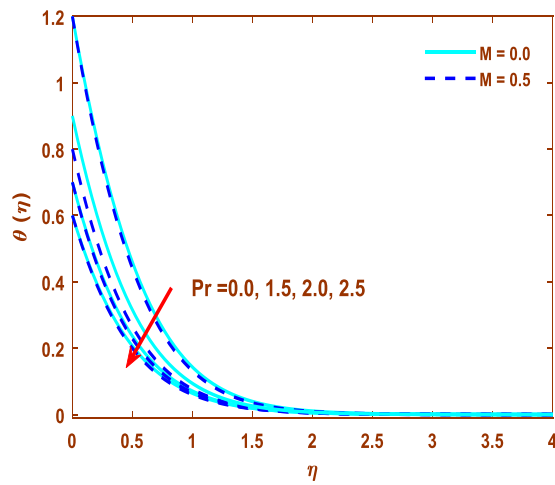


FIGURE 9 $\theta(\eta)$ associated numerically with Pr [Color figure can be viewed at wileyonlinelibrary.com]

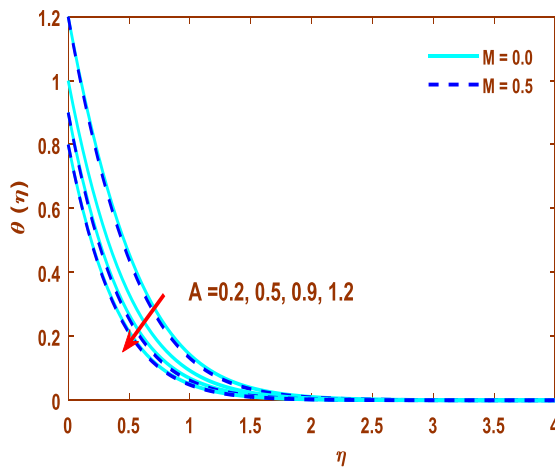


FIGURE 10 $\theta(\eta)$ associated numerically with A [Color figure can be viewed at wileyonlinelibrary.com]

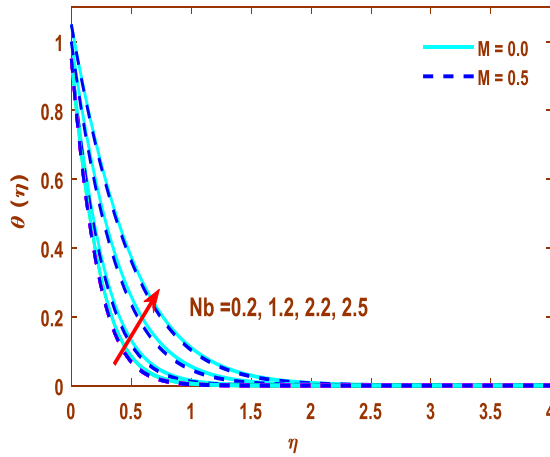


FIGURE 11 $\theta(\eta)$ associated numerically with Nb [Color figure can be viewed at wileyonlinelibrary.com]

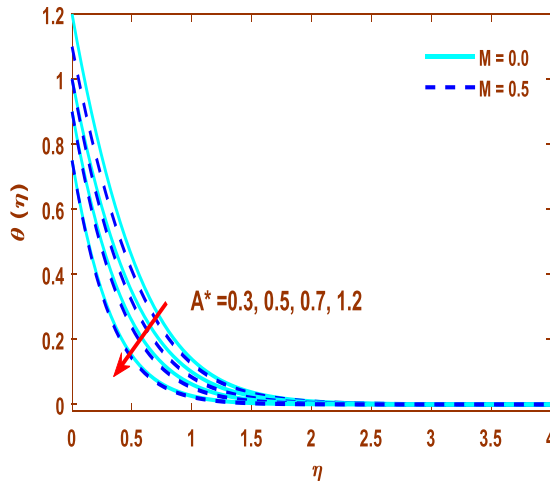


FIGURE 12 $\theta(\eta)$ associated numerically with A^* [Color figure can be viewed at wileyonlinelibrary.com]

constant, and it takes a duration for recovery of fluid after deformation when removal force is present so when it takes stronger numerical values, relaxation of fluid flow becomes stronger, due to this reason, velocity tendency of Carreau nanofluid becomes slow. Figure 2 is evidence of this. The magnetic field generates Lorentz force increasingly from inclined magnetic field to perpendicular magnetic field, due to this Lorentz force is produced accordingly, and as a result velocity tendency of Carreau nanofluid becomes lower. Figure 3 is a pictorial representation of this fact. Carreau nanofluid index n gives a larger velocity, which is shown in Figure 4. Magnetic parameter brings Lorentz force effect, this causes velocity tendency of Carreau nanofluid to become lower and is shown in Figure 5. Temperature is raised by infinite shear rate parameter, so this fact has its influence on velocity tendency of Carreau nanofluid and makes this higher. Geometrically this is represented in Figure 6. Growth in wedge angle parameter β expansion in wedge occurs, due to this expansion velocity tendency of Carreau nanofluid becomes higher, and increasing Unsteadiness parameter gives lower velocity. These facts are established by Figures 7 and 8.

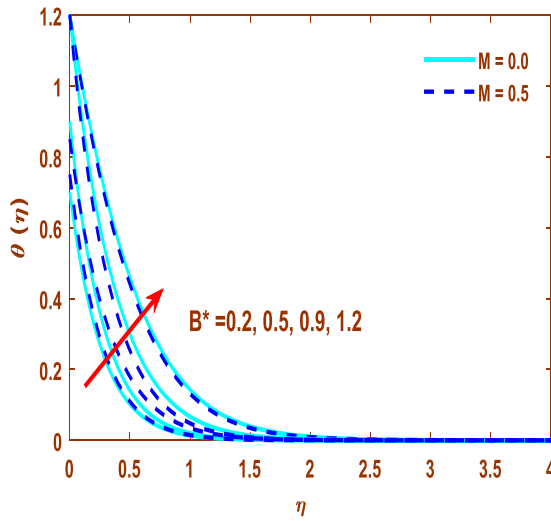
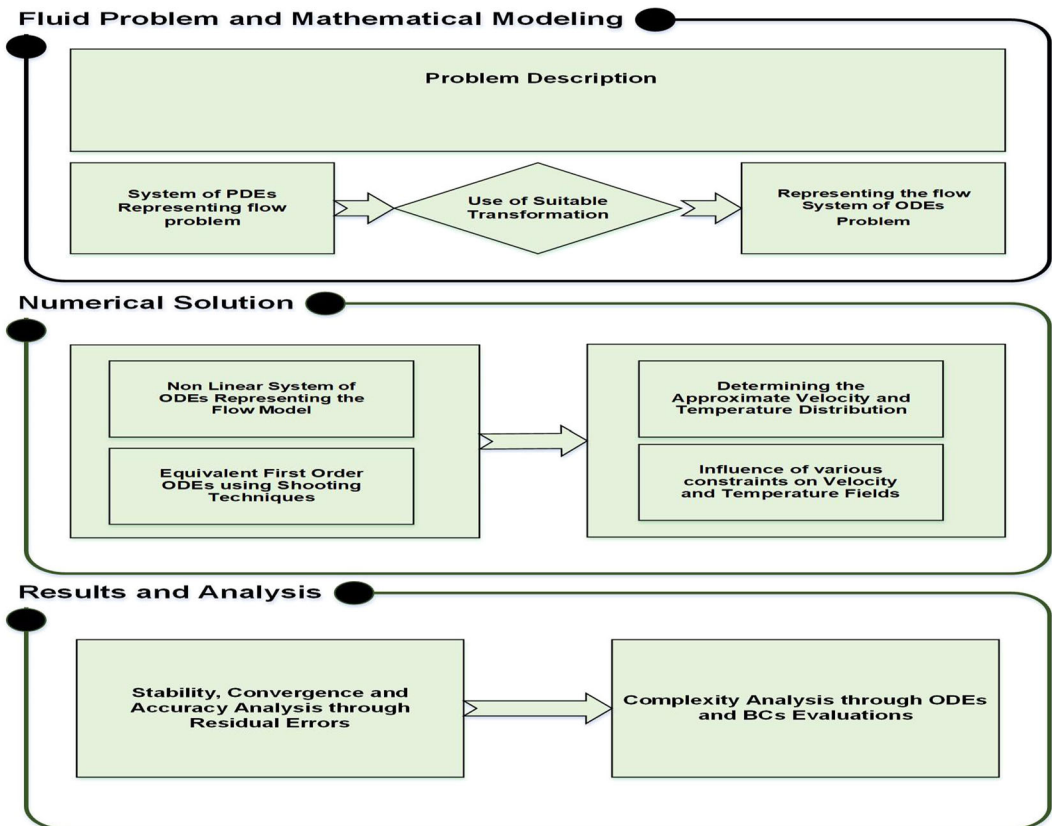


FIGURE 13 $\theta(\eta)$ associated numerically with B^* [Color figure can be viewed at wileyonlinelibrary.com]



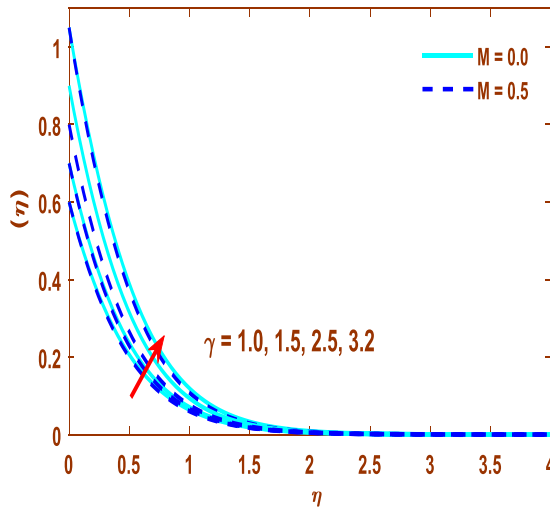


FIGURE 14 $\theta(\eta)$ associated numerically with γ [Color figure can be viewed at wileyonlinelibrary.com]

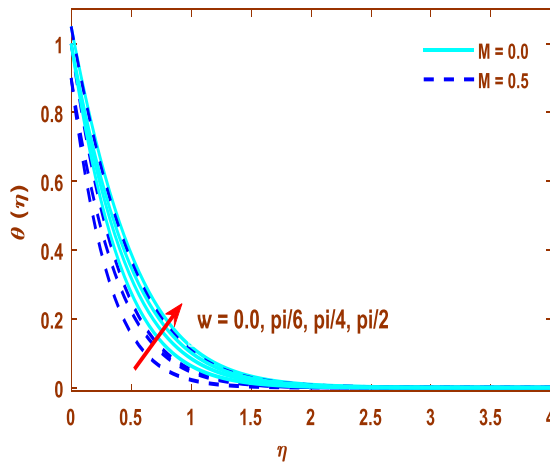


FIGURE 15 $\theta(\eta)$ associated numerically with ω [Color figure can be viewed at wileyonlinelibrary.com]

6.2 | Temperature interpretation of Carreau fluid along seized parameters

The influential contribution of dimensionless parameters on energy profile ($\theta(\eta)$) considering the two cases bearing $M = 0.5$ and absence ($M = 0.0$) is presented in Figures 9–16. From Figure 9, it is clear that Pr causes to lower the thermal diffusivity, due to this energy profile of Carreau nanofluid disintegrates in bearing $M = 0.5$ and absence ($M = 0.0$). Figure 10 depicts that by uplifting the numerical value of A temperature of the sheet becomes low for bearing $M = 0.5$ and absence ($M = 0.0$). Numerical increment in Nb shows the same behavior and geometrically its representation is seen in Figure 11. Figures 12 and 13 are launched to present the influence of the positive value of A^* , B^* on the energy profile of Carreau nanofluid for both cases (presence $M = 0.5$ and absence [$M = 0.0$]). The positive values of A^* , B^* generates internal heat and as a result, the energy profile of

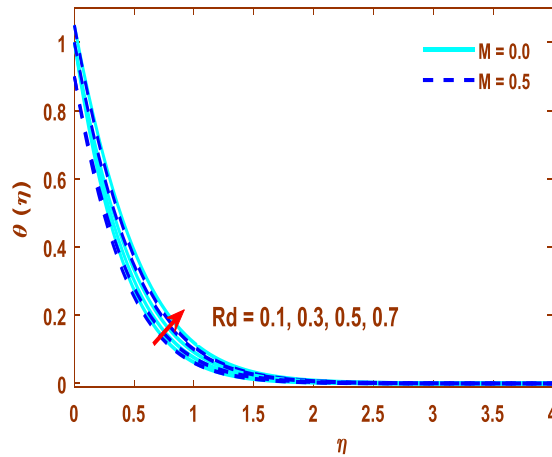


FIGURE 16 $\theta(\eta)$ associated numerically with Rd [Color figure can be viewed at wileyonlinelibrary.com]

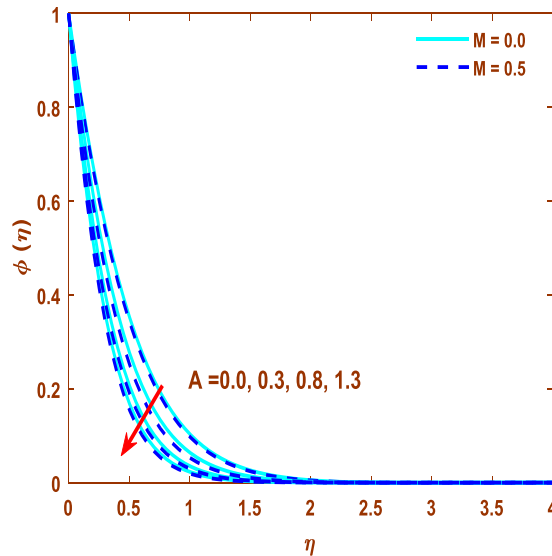


FIGURE 17 $\phi(\eta)$ associated numerically with A [Color figure can be viewed at wileyonlinelibrary.com]

Carreau nanofluid gets rapid. Figures 15 and 16 are placed to give a glimpse to the reader about radiation and inclined angle over energy profile of Carreau nanofluid for both cases. Stronger radiation increases the energy profile of Carreau nanofluid.

6.3 | Nanoparticle concentration interpretation of Carreau fluid along seized parameters

The absence and presence of magnetic parameters have an influence on concentration profiles like velocity and temperature. The influence of concerned parameters with mass transfer

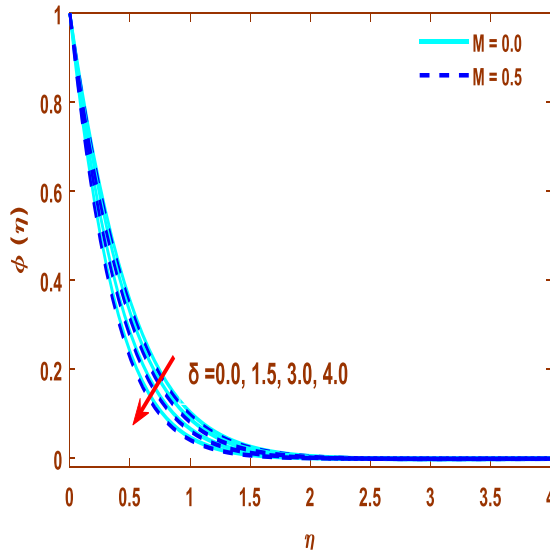


FIGURE 18 $\phi(\eta)$ associated numerically with δ [Color figure can be viewed at wileyonlinelibrary.com]

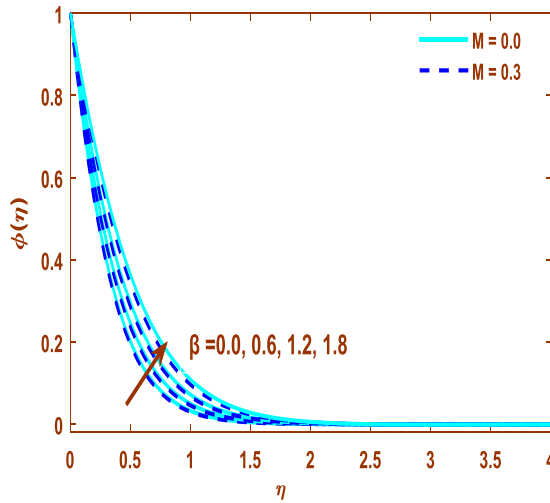


FIGURE 19 $\phi(\eta)$ associated numerically with β [Color figure can be viewed at wileyonlinelibrary.com]

profile is shown in Figures 17–21. Uplifting the numerical values of A boundary layer thickness loses, due to this fact transport of mass is minimized in the presence and absence of a magnetic effect. Boosting the value of δ , a decrement in concentration profile is seen. Moving the wedge angle causes lower concentration. All of these facts are shown in Figures 17–19. Figures 20 and 21 establish the key behavior of Lewis number and inclined angle.

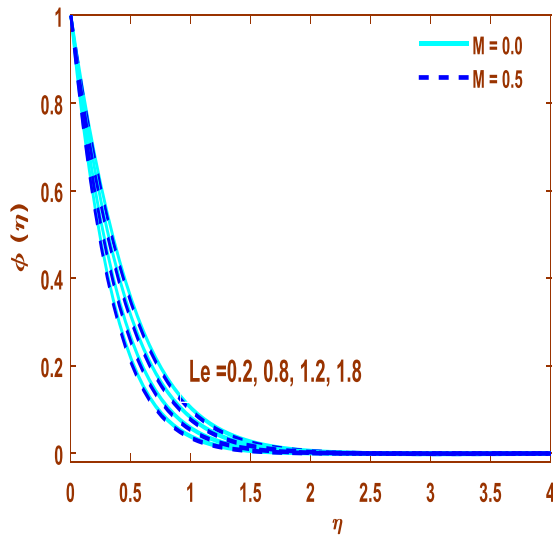


FIGURE 20 $\varphi(\eta)$ associated numerically with Le [Color figure can be viewed at wileyonlinelibrary.com]

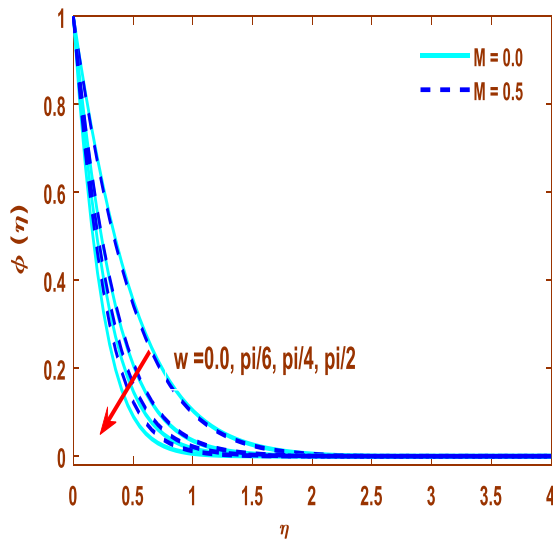


FIGURE 21 $\varphi(\eta)$ associated numerically with ω [Color figure can be viewed at wileyonlinelibrary.com]

6.4 | Reaction of physical quantities and their interpretation for carreau fluid along seized parameters

Real-time physical quantities are incorporated in this section through Figures 22–36. This portion unfolds major key announcement regarding influential parameters (We , β , β^* , A , Ha , ω , Nt , Nb , Pr) on drag force (skin friction), Nusselt number rate of energy transport, and Sherwood number (rate of mass transport). Major findings are a larger value of We and A responses lower velocity so drag force increase, but it reduces for β and β^* .

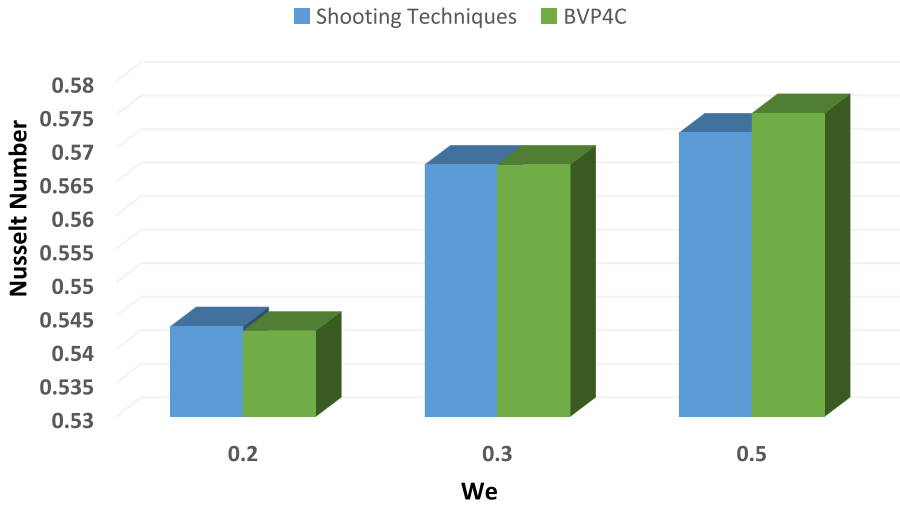


FIGURE 22 $\varphi(\eta)$ associated numerically with We [Color figure can be viewed at wileyonlinelibrary.com]

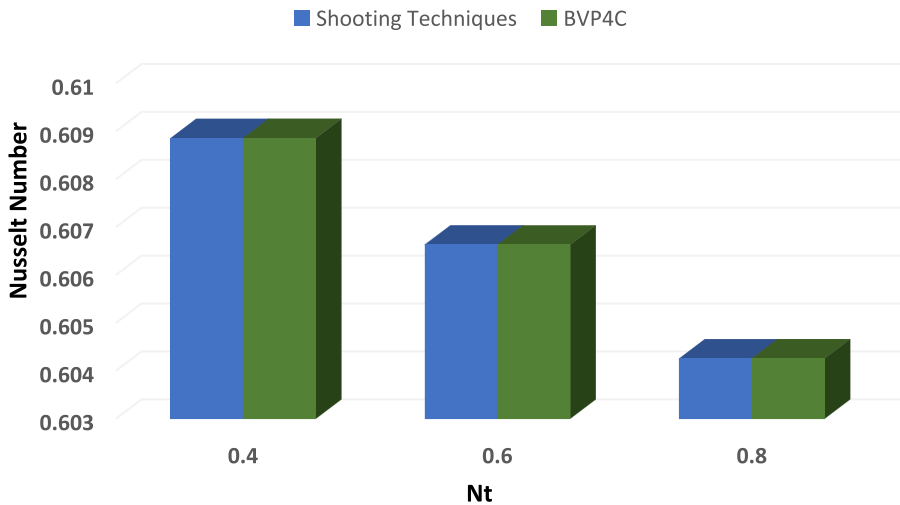


FIGURE 23 $\varphi(\eta)$ associated numerically with Nt [Color figure can be viewed at wileyonlinelibrary.com]

Parameter Nt , β , and Pr cause to lower rate of mass transport, when the angle of the inclined magnetic field is growing then the drag force loses. The rest of the parameters are shown clearly from the geometry.

7 | CONSEQUENCES OF ATTEMPT

This attempt reveals energy exchange with the infinite shear rate viscosity model of Carreau nanofluid by placing inclined magnetic dipole over the wedge. Transportation of heat is launched by utilizing the tools of radiation, Brownian motion, nonuniform heat

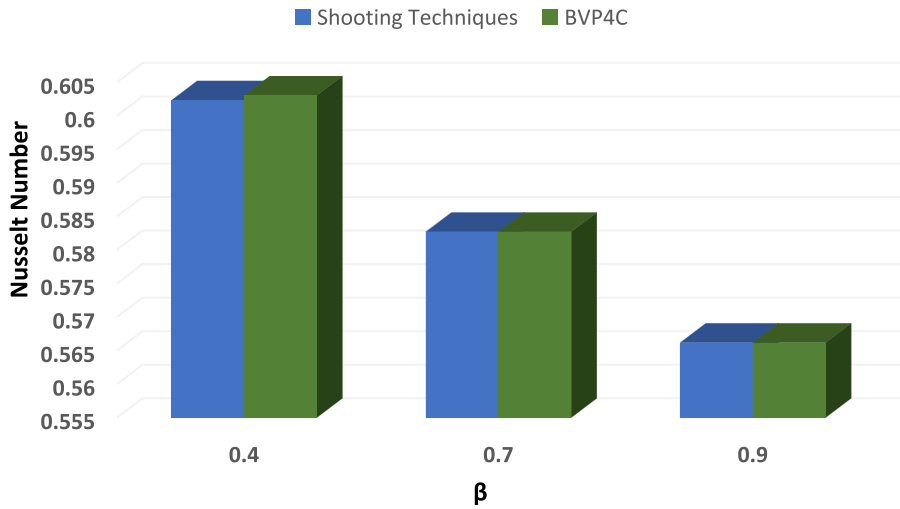


FIGURE 24 Nusselt number associated numerically with β [Color figure can be viewed at wileyonlinelibrary.com]

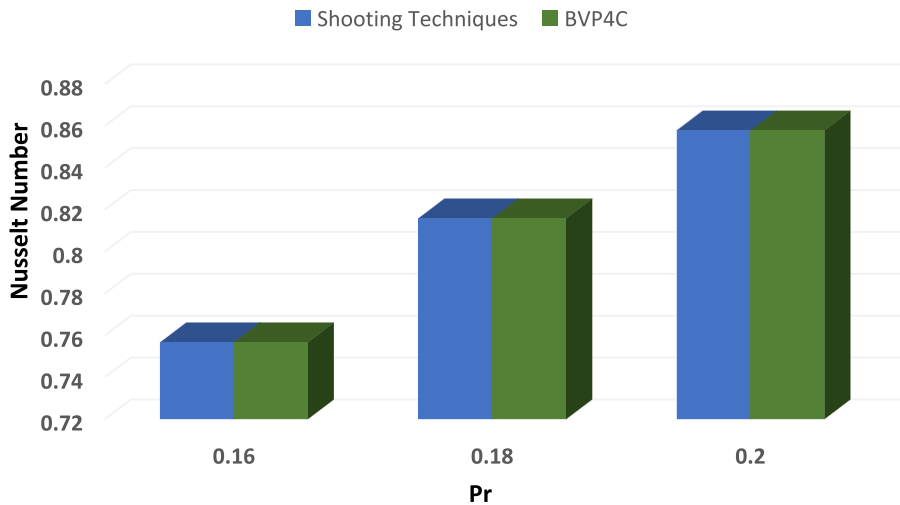


FIGURE 25 Nusselt number associated numerically with Pr [Color figure can be viewed at wileyonlinelibrary.com]

sink source, thermophoresis, and chemical reaction. Mathematical system PDEs are displaced into ODEs and further shooting/Bvp4c numerical procedure is applied to get numerical results.

The number-wise gist of the study is as follows.

1. Inclined magnetic dipole gives a lower velocity of Carreau nanofluid.
2. Due to the relaxation time factor, the velocity of the Carreau fluid gets down.

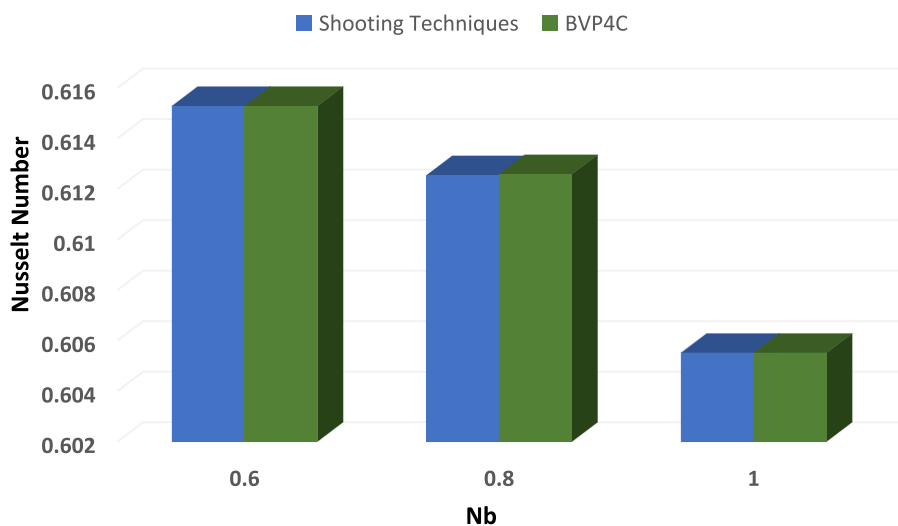


FIGURE 26 Nusselt number associated numerically with Nb [Color figure can be viewed at wileyonlinelibrary.com]

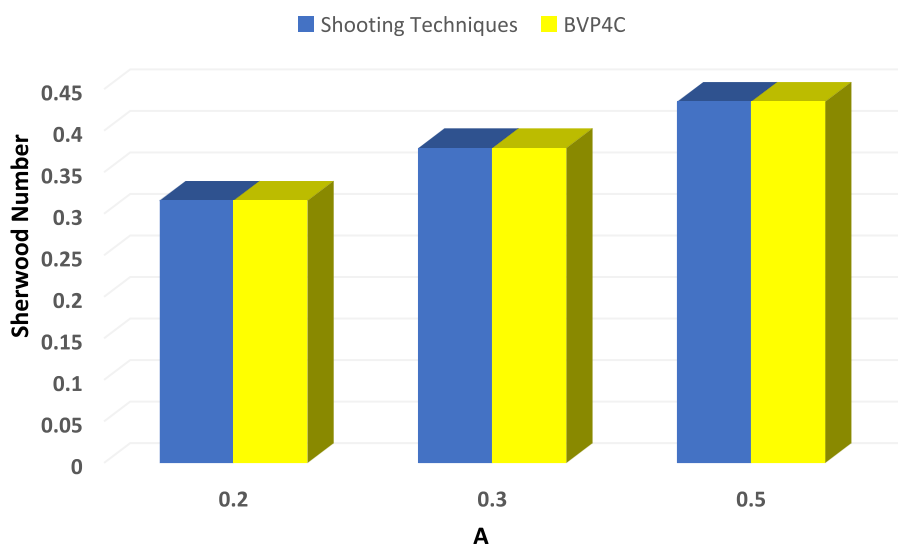


FIGURE 27 Sherwood number associated numerically with A [Color figure can be viewed at wileyonlinelibrary.com]

3. The absence and presence of Magnetic numbers have no influence on velocity, temperature, and concentration files for $Le, R_d, \theta_f, \gamma, We, \beta, Pr, Ha^2, Nb, Nt, A$.
4. An increasing rate of temperature is found very high for the growing Hartmann number.
5. An increment in A^* numerically produces energy internally, due to this temperature increases rapidly.

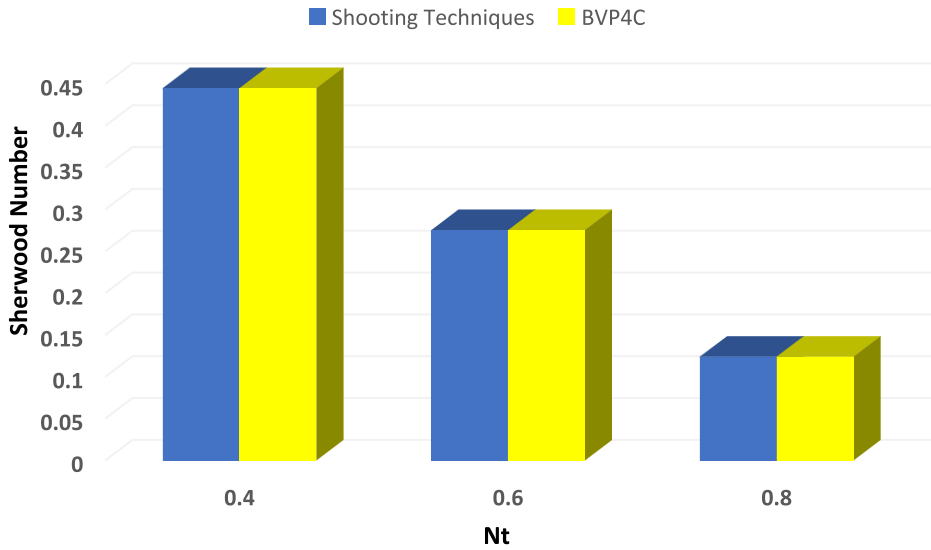


FIGURE 28 Sherwood number associated numerically with Nt [Color figure can be viewed at wileyonlinelibrary.com]

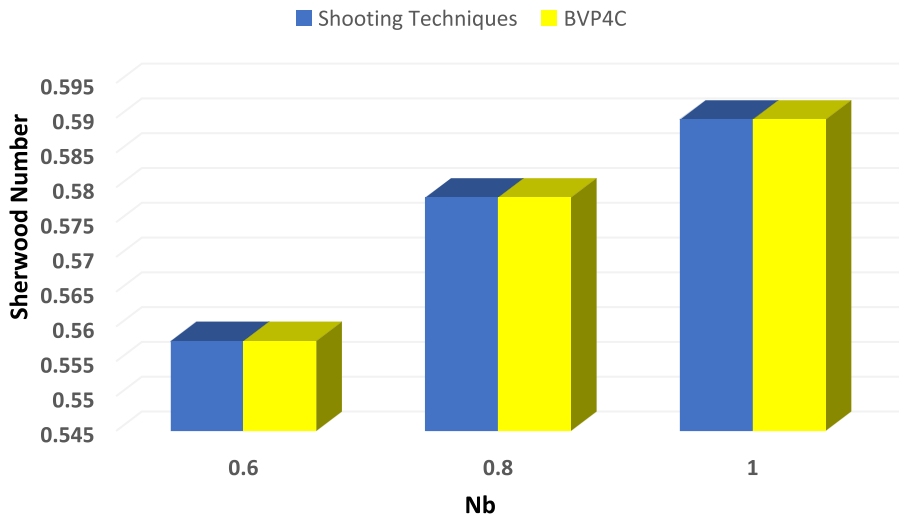


FIGURE 29 Sherwood number associated numerically with Nb [Color figure can be viewed at wileyonlinelibrary.com]

6. Drag force reduces for β and β^* .
7. Growth in parameters noted as β , Pr , and Nt causes to reduce the mass transport of Carreau fluid.
8. Whenever the angle of the inclined magnetic field is going toward the perpendicular, Lorentz's force becomes stronger, and as a result, the drag force loses its magnitude.

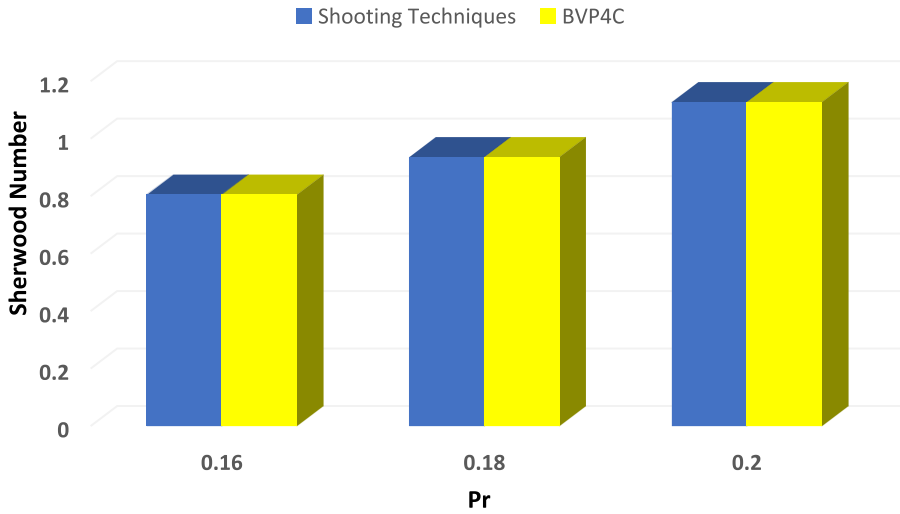


FIGURE 30 Sherwood number associated numerically with Pr [Color figure can be viewed at wileyonlinelibrary.com]

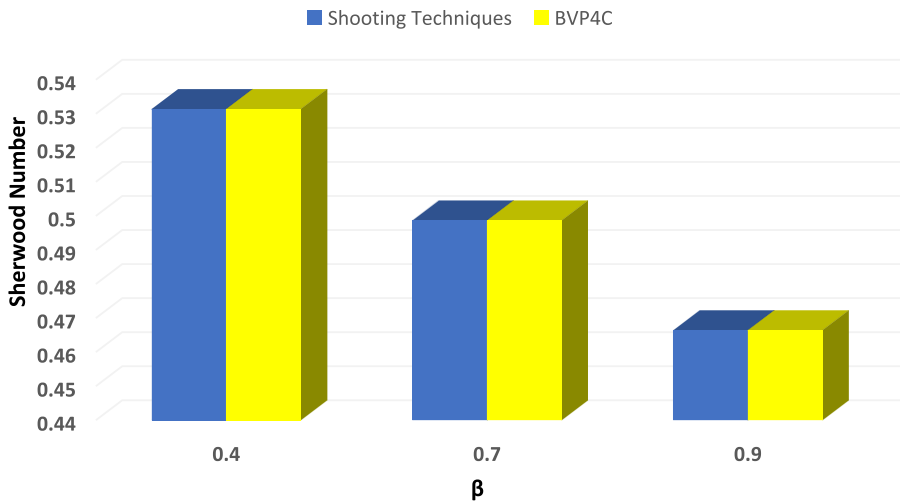


FIGURE 31 Sherwood number associated numerically with β [Color figure can be viewed at wileyonlinelibrary.com]

NOMENCLATURE

- p pressure related to fluid flow
- n Carreau fluid index for shear thinning/thickening
- B inclined magnetic field
- k property of conductivity related to fluid
- τ ratio parameter of two types of heat
- C concentration profile of considered fluid
- T temperature profile of considered fluid

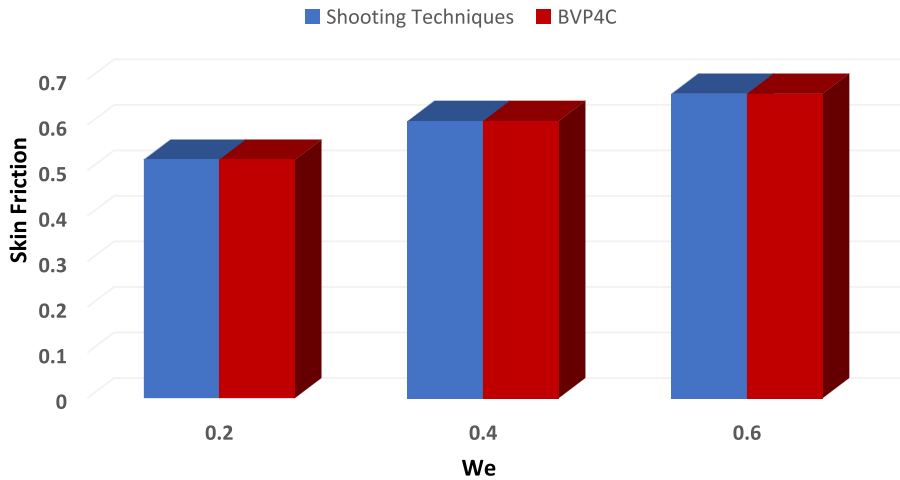


FIGURE 32 Skin friction associated numerically with We [Color figure can be viewed at wileyonlinelibrary.com]

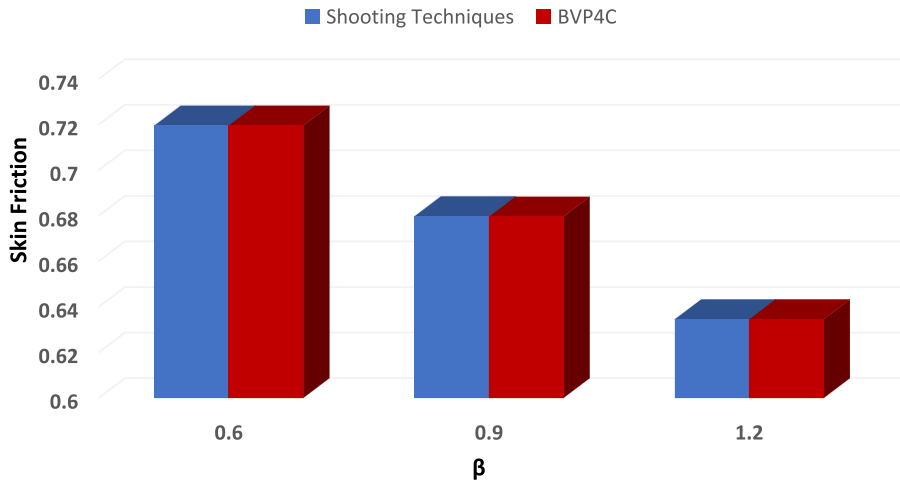


FIGURE 33 Skin friction associated numerically with β [Color figure can be viewed at wileyonlinelibrary.com]

D_B

coefficient related to Brownian motion

$$Ha^2 = \frac{\rho B_0^2}{\rho a x^{m-1}}$$

Hartmann number

D_T

thermophoresis coefficient related to fluid flow

T_∞

infinite temperature measuring for fluid away from wedge

T_f

temperature of the plate or surface of wedge

ω

angle of inclined magnetic field

ρ_f

fluid density

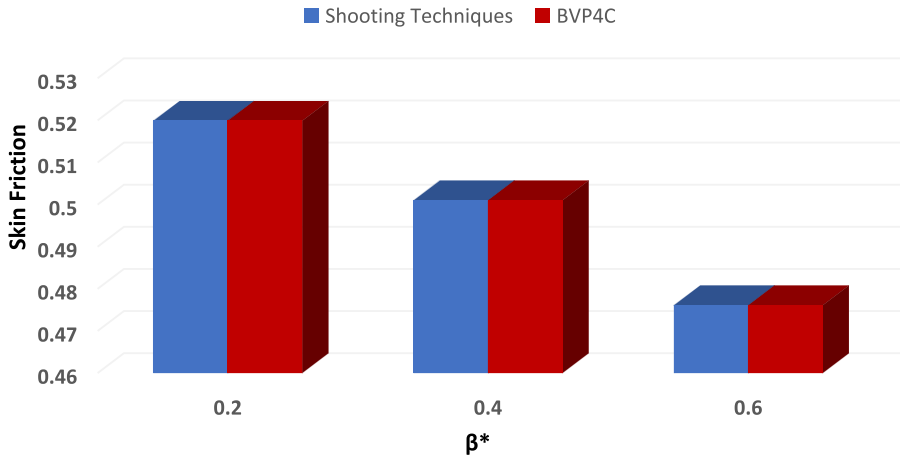


FIGURE 34 Skin friction associated numerically with β^* [Color figure can be viewed at wileyonlinelibrary.com]

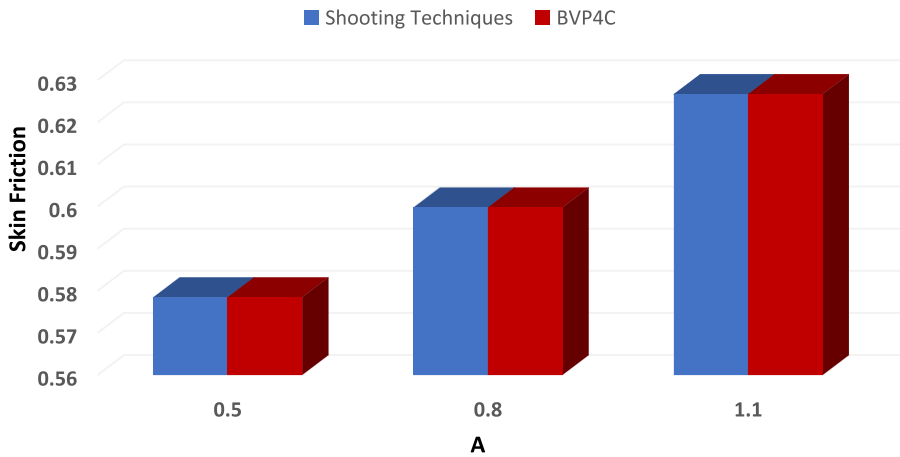


FIGURE 35 Skin friction associated numerically with A [Color figure can be viewed at wileyonlinelibrary.com]

- $\gamma = \frac{h_f}{k} \chi R e^{\frac{1}{2}}$ thermal Biot parameter
- α thermal diffusivity
- c_p specific heat
- M magnetic parameter
- A^* internal heat generation coefficient
- B^* heat sink source parameter
- $\delta = \frac{\sqrt{2} v (C_w - C_\infty)}{\sqrt{m+1}}$ reaction rate parameter
- $A = \frac{c}{ax^{m-1}}$ $\beta = \frac{2m}{m+1}$
- u, v velocity component

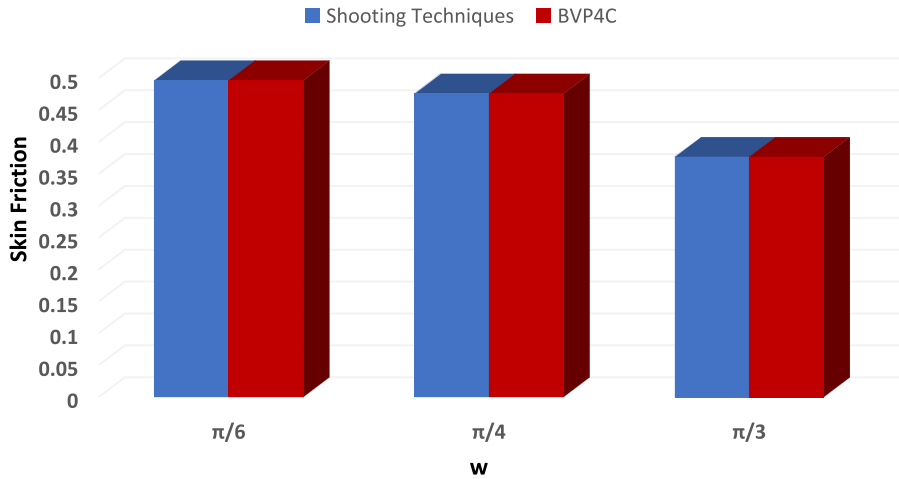


FIGURE 36 Skin friction associated numerically with ω [Color figure can be viewed at wileyonlinelibrary.com]

x, y	space coordinates
σ^*, k^*	Stefan–Boltzmann constant
$Pr = \frac{\nu}{\alpha}$	Prandtl number
$Nb = \frac{\tau D_B (C_w - C_\infty)}{\nu}$	Brownian motion parameter
$Nt = \frac{\tau D_T (T_w - T_\infty)}{\nu T_\infty}$	thermophoresis parameter
$Le = \frac{\alpha}{D_B}$	Lewis number
$We = \sqrt{\frac{\Gamma^2 (m+1) U_e^3}{2\nu x}}$	local Weissenberg number
$\theta_f = \frac{T_w}{T_\infty}$	temperature ratio parameter
U_w, U_∞	stretching velocities
$R_d = \frac{32\sigma^* T_\infty}{6k^* k_\infty}$	radiation parameter
ν	kinematic viscosity
c_f	skin-friction coefficient
N_{ux}	Nusselt number
R_{ex}	local Reynold number
Sh_x	Sherwood number
σ^*	reaction rate of electricity
λ	velocity ratio parameter
k_c	chemical reaction constant
$\alpha = \frac{U_w}{U_e}$	

CONFLICT OF INTERESTS

The authors declare that there are no conflict of interests.

DATA AVAILABILITY STATEMENT

Data are available on request from the authors.

ORCID

Syed Zahir Hussain Shah  <http://orcid.org/0000-0001-6085-0275>

Assad Ayub  <http://orcid.org/0000-0001-9956-6730>

Gilder Cieza Altamirano  <http://orcid.org/0000-0002-7936-1495>

REFERENCES

1. Alam MI, Raj A, Khan PM, Kumar S, Roy S. Numerical simulation of flow of a shear-thinning Carreau fluid over a transversely oscillating cylinder. *J Fluid Mech.* 2021;921.
2. Maqbool K, Manzoor N, Ellahi R, Sait SM. Influence of heat transfer on MHD Carreau fluid flow due to motile cilia in a channel. *J Therm Anal Calorim.* 2021;144(6):2317-2326.
3. Salahuddin T, Awais M, Xia WF. Variable thermo-physical characteristics of Carreau fluid flow by means of stretchable paraboloid surface with activation energy and heat generation. *Case Stud Therm Eng.* 2021; 25:100971.
4. Khan M, Hussain A, Malik MY, Salahuddin T, Aly S. Numerical analysis of Carreau fluid flow for generalized Fourier's and Fick's laws. *Appl Numer Math.* 2019;144:100-117.
5. Ramadevi B, Sugunamma V, Kumar A, JV RR. MHD flow of Carreau fluid over a variable thickness melting surface subject to Cattaneo-Christov heat flux. *Multidiscipl Model Mater Struct.* 2019.
6. Nazir U, Saleem S, Nawaz M, Sadiq MA, Alderremy AA. Study of transport phenomenon in Carreau fluid using Cattaneo-Christov heat flux model with temperature dependent diffusion coefficients. *Physica A: Statist Mech Its Appl.* 2020;554:123921.
7. Khan M, Shahid A, Salahuddin T, Malik MY, Hussain A. Analysis of two dimensional Carreau fluid flow due to normal surface condition: a generalized Fourier's and Fick's laws. *Physica A: Statist Mech Its Appl.* 2020;540:123024.
8. Bhatti MM, Phali L, Khaliq CM. Heat transfer effects on electro-magnetohydrodynamic Carreau fluid flow between two micro-parallel plates with Darcy-Brinkman-Forchheimer medium. *Arch Appl Mech.* 2021;91(4):1683-1695.
9. Afzal Q, Akram S. Impact of double-diffusivity convection in nanofluids and induced magnetic field on peristaltic pumping of a Carreau fluid in a tapered channel with different waveforms. *J Therm Anal Calorim.* 2021;143:2291-2312.
10. Ayub A, Wahab HA, Hussain Shah SZ, Shah SL, Sabir Z, Bhatti S. On heated surface transport of heat bearing thermal radiation and MHD Cross flow with effects of nonuniform heat sink/source and buoyancy opposing/assisting flow. *Heat Transfer.* 2021;50(6):6110-6128.
11. Ayub A, Darvesh A, Altamirano GC, Sabir Z. Nanoscale energy transport of inclined magnetized 3D hybrid nanofluid with Lobatto IIIA scheme. *Heat Transfer.* 2021;50(7):6465-6490.
12. Ayub A, Sabir Z, Le DN, Aly AA. Nanoscale heat and mass transport of magnetized 3-D chemically radiative hybrid nanofluid with orthogonal/inclined magnetic field along rotating sheet. *Case Stud Therm Eng.* 2021;26:101193.
13. Ayub A, Wahab HA, Shah SZ, et al. Interpretation of infinite shear rate viscosity and a nonuniform heat sink/source on a 3D radiative cross nanofluid with buoyancy assisting/opposing flow. *Heat Transfer.* 2021; 50(5):4192-4232.
14. Ayub A, Sabir Z, Altamirano GC, Sadat R, Ali MR. Characteristics of melting heat transport of blood with time-dependent cross-nanofluid model using Keller-Box and BVP4C method. *Eng Comput.* 2021. doi:10.1007/s00366-021-01406-7
15. Guerrero Sánchez Y, Sabir Z, Günerhan H, Baskonus HM. Analytical and approximate solutions of a novel nervous stomach mathematical model. *Discrete Dyn Nature Society.* 2020;2020:2020-2029.

16. Adel W, Sabir Z. Solving a new design of nonlinear second-order Lane–Emden pantograph delay differential model via Bernoulli collocation method. *The Eur Phys J Plus*. 2020;135(5):427.
17. Sabir Z, Günerhan H, Guirao JL. On a new model based on third-order nonlinear multisingular functional differential equations. *Math Probl Eng*. 2020;2020:1683961.
18. Sabir Z, Guirao JL, Saeed T. Solving a novel designed second order nonlinear Lane–Emden delay differential model using the heuristic techniques. *Appl Soft Comput*. 2021;102:107105.
19. Elsonbaty A, Sabir Z, Ramaswamy R, Adel W. Dynamical analysis of a novel discrete fractional sitrs model for COVID-19. *Fractals*. 2021:2140035. doi:10.1142/S0218348X21400351
20. Sabir Z, Ayub A, Guirao JL, Bhatti S, Shah SZH. The effects of activation energy and thermophoretic diffusion of nanoparticles on steady micropolar fluid along with Brownian motion. *Adv Mater Sci Eng*. 2020;2020:2010568.
21. Wahab HA, Hussain Shah SZ, Ayub A, Sabir Z, Bilal M, Altamirano GC. Multiple characteristics of three-dimensional radiative Cross fluid with velocity slip and inclined magnetic field over a stretching sheet. *Heat Transfer*. 2021;50(4):3325-3341.
22. Ayub A, Hafiz AW, Sabir Z, Adnène A. A note on heat transport with aspect of magnetic dipole and higher order chemical process for steady micropolar fluid. *Fluid-Structure Interaction*. IntechOpen; 2020.
23. Shah SZ, Wahab HA, Ayub A, Sabir Z, haider A, Shah SL. Higher order chemical process with heat transport of magnetized cross nanofluid over wedge geometry. *Heat Transfer*. 2021;50(4):3196-3219.
24. Syed Zahir HS, Assad A, Zulqurnain S, Waleed A, Nehad Ali S, Se-Jin Y. Insight into the dynamics of time-dependent cross nanofluid on a melting surface subject to cubic autocatalysis. *Case Stud Therm Eng*. 2021; 27:101227. doi:10.1016/j.csite.2021.101227
25. Sánchez YG, Sabir Z, Guirao JL. Design of a nonlinear SITR fractal model based on the dynamics of a novel coronavirus (COVID-19). *Fractals*. 2020;28(08):2040026.
26. Sabir Z, Sakar MG, Yeskindirova M, Saldir O. Numerical investigations to design a novel model based on the fifth order system of Emden–Fowler equations. *Theor Appl Mech Lett*. 2020;10(5):333-342.
27. Guirao JL, Sabir Z, Saeed T. Design and numerical solutions of a novel third-order nonlinear Emden–Fowler delay differential model. *Math Prob Eng*. 2020;18:2020-5308.
28. Sajid T, Tanveer S, Munsab M, Sabir Z. Impact of oxytactic microorganisms and variable species diffusivity on blood-gold Reiner–Philippoff nanofluid. *Appl Nanosci*. 2021;11(1):321-333.
29. Abdelkawy MA, Sabir Z, Guirao JL, Saeed T. Numerical investigations of a new singular second-order nonlinear coupled functional Lane–Emden model. *Open Phys*. 2020;18(1):770-778.
30. Abbas T, Rehman S, Shah RA, Idrees M, Qayyum M. Analysis of MHD Carreau fluid flow over a stretching permeable sheet with variable viscosity and thermal conductivity. *Physica A: Statist Mech Its Appl*. 2020; 551:124225.
31. Madhu M, Mahanthesh B, Shashikumar NS, Shehzad SA, Khan SU, Gireesha BJ. Performance of second law in Carreau fluid flow by an inclined microchannel with radiative heated convective condition. *Int Commun Heat Mass Transfer*. 2020;117:104761.
32. Khan M, Salahuddin T, Malik MY, Khan F. Change in internal energy of Carreau fluid flow along with Ohmic heating: a Von Karman application. *Physica A: Statist Mech Its Appl*. 2020;547:123440.
33. Mahanthesh B. Magneto hydrodynamic flow of Carreau liquid over a stretchable sheet with a variable thickness: the biomedical applications. *Multidiscipl Model Mater Struct*. 2020;16:1277-1293.
34. Irfan M. Study of Brownian motion and thermophoretic diffusion on non-linear mixed convection flow of Carreau nanofluid subject to variable properties. *Surf Interfaces*. 2021;23:100926.
35. Gowda RP, Kumar RN, Prasannakumara BC, Nagaraja B, Gireesha BJ. Exploring magnetic dipole contribution on ferromagnetic nanofluid flow over a stretching sheet: an application of Stefan blowing. *J Mol Liq*. 2021;335:116215.
36. Shah Z, Dawar A, Islam S. Influence of Brownian motion and thermophoresis parameters on silver-based di-hydrogen CNTs between two stretchable rotating disks. *Phys Scr*. 2021;96(5):055205.
37. Ali B, Pattnaik PK, Naqvi RA, Waqas H, Hussain S. Brownian motion and thermophoresis effects on bioconvection of rotating Maxwell nanofluid over a Riga plate with Arrhenius activation energy and Cattaneo–Christov heat flux theory. *Therm Sci Eng Progr*. 2021;23:100863.

38. Sabir Z, Wahab HA, Umar M, Erdoğan F. Stochastic numerical approach for solving second order non-linear singular functional differential equation. *Appl Math Comput.* 2019;363:124605.
39. Sabir Z, Akhtar R, Zhiyu Z, et al. A computational analysis of two-phase Casson nanofluid passing a stretching sheet using chemical reactions and gyrotactic microorganisms. *Math Prob Eng.* 2019;2019:1490571.

How to cite this article: Shah SZH, Fathurrochman I, Ayub A, et al. Inclined magnetized and energy transportation aspect of infinite shear rate viscosity model of Carreau nanofluid with multiple features over wedge geometry. *Heat Transfer.* 2021;1-27. doi:10.1002/htj.22367